Progress In Electromagnetics Research B, Vol. 86, 39–57, 2020

Numerical Modelling of Electro-Magnetohydrodynamic Disturbances (E-MHD) in a Two-Dimensional Configuration in the Vertical Plane in the Ionosphere: Small Scale and Medium Scale Ionospheric Disturbances

Victor Nijimbere* **and Lucy J. Campbell**

Abstract—We have simulated ionospheric disturbances generated by the buoyancy and electrodynamic effects in a two-dimensional configuration in the vertical plane in the ionospheric F region using a simple two-dimensional mathematical model for internal gravity waves propagating in the lower atmosphere, and we have investigated the characteristics (e.g., buyoancy frequency, wavenumber, wavelength, speed) of the ionospheric disturbances. We find that electrohydrodynamic effects are mainly responsible for small scale non-travelling ionospheric disturbances, while magnetohydrodynamic effects are responsible for travelling ionospheric disturbances, including small scale travelling ionospheric disturbances (SSTIDs), medium scale travelling ionospheric disturbances (MSTIDs) and large scale travelling ionospheric disturbances (LSTIDs). Our results are in agreement with the results obtained from observations.

1. INTRODUCTION

The Earth's ionosphere, the region in the upper atmosphere, contains electrons and ions resulting from the effects of the ultraviolet and X-ray radiation from the sun which contains enough energy to remove electrons from the gases in the ionosphere. The density of electrons can significantly affect radio wave propagation, and consequently the ability to transmit radio waves over long distances and receive signals, see for example [12, 18]. Radio waves interact with the ionosphere via reflection and refraction from one layer to another, wave diffraction over obstacles and wave scattering [12].

The ionosphere is subdivided into three main regions, the lower region D extending from an altitude of about 40 km to 90 km with an electron number density $\approx 2.5 \times 10^9\,\mathrm{m}^{-3}$, E extending from an altitude of about 90 km to 160 km with an electron number density $\approx 2 \times 10^{11}\,\mathrm{m}^{-3}$, and above the E region, the F region extends to an altitude of more than 800 km with an electron number density $\approx 2.5 \times 10^{12}\,\mathrm{m}^{-3}$. The F region is strongly magnetized, and most high frequency radio waves of order of GHz are reflected in this region of the ionosphere.

When there are solar winds, e.g., magnetic storms, and other phenomena that transport random scatters and perturb the geomagnetic field, their interactions with the ionospheric medium occur in a random fashion and often generate ionospheric disturbances (waves) and electromagnetic waves, see [1, 2, 5, 6, 13, 24] and references therein. Ionospheric disturbances comprise large scale travelling ionospheric disturbances (LSTIDs) with horizontal wavelength longer than 1000 km propagating at a speed greater than $300\,\mathrm{m\ sec}^{-1}$, medium scale travelling ionospheric disturbances (MSTIDs) with horizontal wavelength longer than 100 km propagating at a speed less than $400\,\mathrm{m\ sec}^{-1}$, and small scale

Received 25 August 2019, Accepted 19 November 2019, Scheduled 9 December 2019
* Corresponding author: Victor Nijimbere (victornijimbere@gmail.com).
The authors are with the School of Mathematics and Statistics, Carleton University, Ottawa, Ontario, Canada.

ionospheric disturbances with wavelength shorter than 100 km [2, 9, 27, 31]. It is also well known that not all small scale ionospheric disturbances are travelling [2, 9, 27].

Downward propagating ionospheric disturbances can reach the lower atmosphere and interact with atmospheric waves and consequently affect the general circulation of the atmosphere and, hence, weather and climate [5, 14, 17, 19]. They can also damage (electric) power grids, avionics and ground systems, GPS and other positioning, navigation and timing (PNT) systems, and radio communication systems (e.g., Mobile satellite communications), and hence cause considerable human and economic losses, see for example [3, 30]. It is thus important for us to understand the properties of the ionosphere in order to ensure effective radio communications and to adequately protect satellites (spatial stations) and astronauts who travel in the ionosphere, electric power grids, avionics and ground systems, and aircraft passengers and crew, and therefore mitigate the losses which may be caused by ionospheric disturbances [3, 6, 25].

Our understanding of the ionosphere can be significantly improved by performing numerical simulations using mathematical models like those used for weather prediction and climate modeling in the lower atmosphere. The fluid dynamics governing equations which are based on the law of conservation of mass, momentum and energy can apply in the ionosphere. However, electrodynamic processes have to be taken into consideration. Furthermore, to take into account the presence of random scatters in the medium, the ionosphere can be considered to be an isotropic medium with weakly-random fluctuations in time as in [22], and thus we can model the ionospheric disturbances in terms of stochastic partial differential equations (SPDEs). Our purpose is to simulate the nonlinear interactions between the electromagnetic field and the medium. Our numerical model will be solved using a numerical method based on the Wiener chaos expansion (WCE) as described in Nijimbere [20, 21].

It was found that electrodynamic processes can play an important role in the variation of the buoyancy effects and hence can generate ionospheric wave-like structures resembling atmospheric (internal) gravity waves [11, 13]. Kelley et al. called these ionospheric wave-like structures electrohydrodynamic waves. These wave structures (or ionospheric disturbances) are mainly generated by the Lorentz force and the Joule heating produced from intensified auroral electrojet and/or intense particle precipitation in the auroral and subauroral regions during geomagnetic storms [7, 11].

In the present study, we investigate ionospheric disturbances (waves) generated via the Lorentz force, and we separately look at the roles of the electrohydrodynamic and magnetohydrodynamic effects. Thus, we categorize these waves into two categories which are electrohydrodynamic disturbances (EHD) generated by the effects due to the electric field and magnetohydrodynamic disturbances (MHD) generated by the effects due to the magnetic field.

We consider that electrodynamic processes play an important role in the variation of the buoyancy force [11, 13]. In that case, a simple two-dimensional mathematical model analogous to that for internal gravity waves [29] propagating in the neutral (lower) atmosphere can be used to model the electro-magnetohydrodynamic (E-MHD) disturbances. It consists of a rectangular domain in a plane perpendicular to the surface of the earth with Cartesian coordinates, x in the horizontal direction and z in the vertical direction, and the waves are considered to be perturbations to some basic background (or mean) flow. The background flow velocity has no vertical component, and its horizontal component is the horizontal mean flow speed, for example it could be represented as

$$\bar{\mathbf{u}} = (\bar{u}(z), 0).$$

This configuration allows mathematical analyses using perturbation theory and both linear and nonlinear numerical simulations. In this study, waves are generated at the upper boundary of the rectangular domain and propagate downward in the negative z-direction toward the Earth. The results of our numerical simulations show that electrohydrodynamic effects are mainly responsible for small scale ionospheric disturbances which are non travelling [9], while magnetohydrodynamic effects are responsible for travelling ionospheric disturbances comprising small scale travelling ionospheric disturbances (SSTIDs), medium scale travelling ionospheric disturbances (MSTIDs) and large scale travelling ionospheric disturbances (LSTIDs).

We organize the paper as follows. The mathematical model in terms of streamfunction, vorticity and density is derived in Section 2. In Section 3, we describe the numerical implementation (the numerical model and boundary conditions), and some results are described in Section 4. A general discussion and some conclusions are given in Section 5.

2. MATHEMATICAL MODELLING

The mathematical model for the ionospheric α-species or plasma consists of the momentum equation

$$\varrho_\alpha \frac{D\mathbf{u}_\alpha}{Dt} = -\nabla p_\alpha + \varrho_\alpha \mathbf{g} + \mu \nabla^2 \mathbf{u}_\alpha + \varrho_{\alpha,el}(\mathbf{E} + \mathbf{u}_\alpha \times \mathbf{B}), \tag{1}$$

the continuity equation

$$\frac{1}{\varrho_\alpha}\frac{D\varrho_\alpha}{Dt} + \nabla \cdot \mathbf{u}_\alpha = \frac{1}{\varrho_\alpha}(Q_\alpha - L_\alpha)M_\alpha, \tag{2}$$

the energy equation in terms of the ionospheric α-species density under Boussinesq approximation (see Appendix A)

$$\frac{D\varrho_\alpha}{Dt} = \mathcal{T}_\alpha \nabla^2 \varrho_\alpha - \frac{\kappa_\alpha}{C_{p,\alpha}} \nabla \cdot (\mathbf{E} \times \mathbf{H}), \tag{3}$$

Maxwell's equations describing the electromagnetic field

$$\nabla \times \mathbf{E} = -\frac{\partial \mathbf{B}}{\partial t}, \tag{4}$$

$$\nabla \times \mathbf{H} = \mathbf{J}_\alpha + \frac{\partial \mathbf{D}}{\partial t}, \tag{5}$$

$$\nabla \cdot \mathbf{D} = \varrho_{\alpha,el}, \tag{6}$$

$$\nabla \cdot \mathbf{B} = 0, \tag{7}$$

and the electric charge of the α species continuity equation

$$\frac{\partial \varrho_{\alpha,el}}{\partial t} = -\nabla \cdot \mathbf{J}_\alpha, \tag{8}$$

where $\mathbf{u}_\alpha = \hat{\mathbf{x}} u_\alpha + \hat{\mathbf{z}} w_\alpha$, ϱ_α, p_α and $\varrho_{\alpha,el}$ are the velocity, the density, the pressure and the electric charge density of the ionospheric α-species (plasma); $\mathbf{g} = -\hat{\mathbf{z}} g, g \approx 9.8\,\mathrm{m\ sec}^{-2}$, is the acceleration due to gravity; Q_α and L_α are production and loss rates of the α-species, respectively; μ_α is the α-species viscosity coefficients; $\mathcal{T}_\alpha$ is the thermal diffusivity; $C_{p,\alpha}$ is a typical specific heat capacity at constant pressure; $\kappa_\alpha \approx 1/T_{\alpha,0}$ is a typical plasma thermal expansion; $T_{\alpha,0}$ is a reference temperature; $\mathbf{E}$ and $\mathbf{H}$ are the electric and magnetic field vectors; $\mathbf{D}$ and $\mathbf{B}$ are electric and magnetic flux densities; $\mathbf{J}_\alpha$ is the current density; $\frac{D}{Dt} = \frac{\partial}{\partial t} + u\frac{\partial}{\partial x} + w\frac{\partial}{\partial z}$ denotes the derivative following the fluid motion; and $\hat{\mathbf{x}}$ and $\hat{\mathbf{z}}$ are unit vectors in the horizontal (west to east) and vertical directions, respectively.

The ideal magnetohydrodynamic (MHD) assumption is commonly used to formulate the MHD equations [8, 15]. It makes use of the expression $\mathbf{E} = -\mathbf{u} \times \mathbf{B}$ for the electric field $\mathbf{E}$ in Maxwell's and energy equations [8, 15]. In that case, $\mathbf{E} + \mathbf{u} \times \mathbf{B} = 0$ in the momentum Equation (1). As a result of this, there is no magnetohydrodynamic problem to solve. To get around these inconsistencies, we consider that the ionosphere is a weakly-dispersive time-dependent linear isotropic medium as in Nijimbere and Campbell [22], and thus, we obtain the expressions for $\mathbf{E}, \mathbf{H}, \mathbf{B}$ and $\varrho_{\alpha,el}$ to substitute in the momentum Equation (1) and in the energy Equation (3).

The vector quantities $\mathbf{E}$ and $\mathbf{D}$, and $\mathbf{H}$ and $\mathbf{B}$ are thus related by

$$\mathbf{D}(\mathbf{r}, t) = \epsilon(t)\mathbf{E}(\mathbf{r}, t) \text{ and } \mathbf{B}(\mathbf{r}, t) = \mu(t)\mathbf{H}(\mathbf{r}, t), \tag{9}$$

where $\epsilon(t)$ and $\mu(t)$ are, respectively, the permittivity and permeability of the medium; $\mathbf{r}$ is the position vector; and each component of $\mathbf{E}$ is the solution of

$$\nabla^2 E - \mu \frac{\partial^2(\epsilon E)}{\partial t^2} - \frac{d\mu}{dt}\frac{\partial(\epsilon E)}{\partial t} = 0 \tag{10}$$

We consider a two-dimensional rectangular domain $x_1 \le x \le x_2$ and $-\infty < z \le z_2$, where x represents the horizontal (west to east) coordinate, and z is the altitude, and we let

$$\mathbf{E}(x, z, t) = \hat{\mathbf{x}} E_x(x, z, t) + \hat{\mathbf{z}} E_z(x, z, t) \text{ and } \mathbf{D}(x, z, t) = \hat{\mathbf{x}} D_x(x, z, t) + \hat{\mathbf{z}} D_z(x, z, t). \tag{11}$$

Electric measurements indicate that, under certain circumstances (e.g., during solar winds), the upper region of the ionosphere, known as the F region, may behave like an electric dynamo with a direct

current electric field [10, 26]. Therefore, we have to carefully choose initial and boundary conditions for Eq. (10) that will give a solution representing a direct current electric field.

Following [22], we solve Eq. (10) subject to the initial conditions

$$E_x(x,z,0) = f(0)\frac{\rho_s e^{\eta_e z}}{\epsilon(0)}\sin(\eta_e x) \text{ and } E_z(x,z,0) = f(0)\frac{\rho_s e^{\eta_v z}}{\epsilon(0)}\cos(\eta_v x),\ x_1 \le x \le x_2,\ -\infty < z \le z_2 \tag{12}$$

and the boundary conditions

$$E_x(x,z_2,t) = f(t)\frac{\rho_s}{\epsilon(t)}\sin(\eta_e x) \text{ and } E_z(x,z_2,t) = f(t)\frac{\rho_s}{\epsilon(t)}\cos(\eta_v x),\ t \ge 0, \tag{13}$$

where

$$f(t) = \begin{cases} 1, \text{ if } t < t_0 \\ 0, \text{ if } t > t_0 \end{cases}, \tag{14}$$

acts as a switch-off of the electromagnetic field source, $t_0 > 0$, and ρ_s is a constant reference surface charge density at the altitude z_1, the source level of the electromagnetic field. Thus, these conditions give the electric field vector solution

$$\mathbf{E}(x,z,t) = \hat{\mathbf{x}}E_x(x,z,t) + \hat{\mathbf{z}}E_z(x,z,t) = \hat{\mathbf{x}}f(t)\frac{\rho_s}{\epsilon(t)}e^{\eta_e(z-z_2)}\sin(\eta_e x) + \hat{\mathbf{z}}f(t)\frac{\rho_s}{\epsilon(t)}e^{\eta_v(z-z_2)}\cos(\eta_v x). \tag{15}$$

Using Eq. (9), we obtain the electric flux density

$$\mathbf{D}(x,z,t) = \hat{\mathbf{x}}\epsilon(t)E_x(x,z,t) + \hat{\mathbf{z}}\epsilon(t)E_z(x,z,t) = \hat{\mathbf{x}}f(t)\rho_s e^{\eta_e(z-z_2)}\sin(\eta_e x) + \hat{\mathbf{z}}f(t)\rho_s e^{\eta_v(z-z_2)}\cos(\eta_v x). \tag{16}$$

Maxwell's Equation (6) gives

$$\varrho_{\alpha,el}(x,z,t) = \nabla\cdot\mathbf{D} = \frac{\partial D_x}{\partial x} + \frac{\partial D_z}{\partial z} = f(t)\left[\eta_e\rho_s e^{\eta_e(z-z_2)}\cos(\eta_e x) + \eta_v\rho_s e^{\eta_v(z-z_2)}\cos(\eta_v x)\right]. \tag{17}$$

The electric charge density $\varrho_{\alpha,el}$ is indeed time-independent prior the electromagnetic field source is switched off. Therefore, the ionosphere acts like an electric dynamo with a direct current. The magnetic flux density is obtained using Maxwell's Equation (4),

$$\begin{aligned}\mathbf{B}(x,z,t) &= -\int \nabla\times\mathbf{E}dt = \hat{\mathbf{y}}B_y = \hat{\mathbf{y}}\int\left(\frac{\partial E_z}{\partial x} - \frac{\partial E_x}{\partial z}\right)dt \\ &= -\hat{\mathbf{y}}f(t)\rho_s\left[\eta_e e^{\eta_e(z-z_2)}\sin(\eta_e x) + \eta_v e^{\eta_v(z-z_2)}\sin(\eta_v x)\right]\int\frac{1}{\epsilon(t)}dt.\end{aligned} \tag{18}$$

In the next section, the momentum equation is written in terms of the streamfunction and the vorticity using the Boussinesq approximation (see Appendix A). Under the Boussinesq approximation, it is assumed that the density slowly varies with time and in space, and so $D\varrho_\alpha/Dt \ll \varrho_\alpha$. We also assume that ϱ_α is large enough so that $(Q_\alpha - L_\alpha)M_\alpha \ll \varrho_\alpha$. This corresponds to a configuration where the production and loss rates of the α species are almost equal ($Q_\alpha \approx L_\alpha$), for example, in the ionospheric F region. In that case, the continuity Equation (2) reduces to

$$\nabla\cdot\mathbf{u}_\alpha = 0. \tag{19}$$

This form of the continuity equation allows us to define the streamfunction for the plasma by

$$-\frac{\partial\Psi_\alpha}{\partial z} = u_\alpha \text{ and } \frac{\partial\Psi_\alpha}{\partial x} = w_\alpha,$$

and the vorticity by

$$\frac{\partial w_\alpha}{\partial x} - \frac{\partial u_\alpha}{\partial z} = \frac{\partial\Psi_\alpha}{\partial x} + \frac{\partial\Psi_\alpha}{\partial z} = \nabla^2\Psi_\alpha.$$

2.1. Streamfunction-Vorticity Formulation

The Lorentz force per unit of electric charge $\mathbf{u}_\alpha \times \mathbf{B}$, where $\mathbf{B}$ is given by Eq. (18), is thus given by

$$\mathbf{u}_\alpha \times \mathbf{B} = (\hat{\mathbf{x}} u_\alpha + \hat{\mathbf{z}} w_\alpha) \times \hat{\mathbf{y}} B_y = -\hat{\mathbf{x}} w_\alpha B_y + \hat{\mathbf{z}} u_\alpha B_y, \tag{20}$$

where B_y is the y-component of the magnetic flux density. Under the Boussinesq approximation (Appendix A), it is assumed that the density is constant except in the buoyancy terms where it multiplies the acceleration due to gravity g. Using the Boussinesq approximation and the fact that the Lorentz force does not have a y-component, the y-component of the momentum Equation (1) can be decoupled from the other two components. Therefore, in two-dimensional Cartesian coordinates in the vertical xz-plane, we have

$$\frac{\partial u_\alpha}{\partial t} + u_\alpha \frac{\partial u_\alpha}{\partial x} + w_\alpha \frac{\partial u_\alpha}{\partial z} = -\frac{1}{\varrho_{\alpha_o}} \frac{\partial p_\alpha}{\partial x} + \nu_\alpha \nabla^2 u_\alpha - \frac{\varrho_{\alpha,el} B_y}{\varrho_{\alpha_o}} w_\alpha + \frac{\varrho_{\alpha,el}}{\varrho_{\alpha_o}} E_x, \tag{21}$$

and

$$\frac{\partial w_\alpha}{\partial t} + u_\alpha \frac{\partial w_\alpha}{\partial x} + w_\alpha \frac{\partial w_\alpha}{\partial z} = -\frac{1}{\varrho_{\alpha_o}} \frac{\partial p_\alpha}{\partial x} - \frac{\varrho_\alpha}{\bar{\rho}_\alpha} g + \nu_\alpha \nabla^2 w_\alpha + \frac{\varrho_{\alpha,el} B_y}{\varrho_{\alpha_o}} u_\alpha + \frac{\varrho_{\alpha,el}}{\varrho_{\alpha_o}} E_z, \tag{22}$$

where the components of the electric field vector E_x and E_z are given by Eq. (15), and the electric charge density $\varrho_{\alpha,el}$ is given by Eq. (17). $\nu_\alpha = \frac{\mu_\alpha}{\varrho_{\alpha_o}}$ is the plasma kinematic viscosity, and ϱ_{α_0} is a constant reference density.

In the ionospheric F region, T_α varies slowly between 1000 and 1500 Kelvin with altitude z and the magnetic storm intensity [33]. Therefore, we are justified to use the Boussinesq approximation [28]. We take into consideration density variations in the term involving the buoyancy force in the momentum Equation (22), i.e., the term multiplied by the acceleration due to gravity g [28]. The vertical gradient $d\bar{\rho}(z)/dz$ is also considered to be small compared with the density $\bar{\rho}(z)$ so that terms in the vertical momentum equation that are proportional to the ratio $(d\bar{\rho}(z)/dz)/\bar{\rho}(z)$ can be neglected in the streamfunction-vorticity formulation. We express the background plasma mean flow density as

$$\bar{\rho}_\alpha(z) = \rho_{\alpha_0}\, e^{-(z-z_1)/H_i}, \tag{23}$$

where $H_i \approx k/(m_\alpha g) T_\alpha$ is the ionospheric scale height; $k = 1.38 \cdot 10^{-23} \mathrm{J} \cdot \mathrm{K}^{-1}$ is Boltzmann constant; m_α is the mass of the α-species; as before, T_α is their temperature; and g is the magnitude of the acceleration due to gravity. The ionospheric (plasma) buoyancy frequency is thus given by

$$N_i^2 = -\frac{g}{\bar{\rho}_\alpha} \frac{d\bar{\rho}_\alpha}{dz} = \frac{g}{H_i}. \tag{24}$$

We now combine Eqs. (21) and (22) and obtain the vorticity equation in terms of the streamfunctions Ψ_α and the vorticity $\nabla^2 \Psi_\alpha$ by differentiating Eq. (21) with respect to z and Eq. (22) with respect x and subtracting one equation from another to eliminate the pressure terms. This gives

$$\begin{aligned} \nabla^2 \Psi_{\alpha_t} - \Psi_{\alpha_z} \nabla^2 \Psi_{\alpha_x} + \Psi_{\alpha_x} \nabla^2 \Psi_{\alpha_z} + g(\bar{\rho}_\alpha)^{-1} \varrho_{\alpha_x} - \nu_\alpha \nabla^4 \Psi_\alpha \\ - (\varrho_{\alpha_0})^{-1} \left[(\varrho_{\alpha,el} B_y)_x \Psi_{\alpha_z} - (\varrho_{\alpha,el} B_y)_z \Psi_{\alpha_x} - (\varrho_{\alpha,el} E_x)_z + (\varrho_{\alpha,el} E_z)_x \right] = 0. \end{aligned} \tag{25}$$

The energy Equation (3) is written in terms of the streamfunction Ψ_α and the plasma density ϱ_α as

$$\varrho_{\alpha_t} - \Psi_{\alpha_z} \varrho_{\alpha_x} + \Psi_{\alpha_x} \varrho_{\alpha_z} - \mathcal{T}_\alpha \nabla^2 \varrho_\alpha = -\frac{\kappa_\alpha}{C_{p,\alpha}} \nabla \cdot (\mathbf{E} \times \mathbf{H}). \tag{26}$$

We perform a numerical study based on a nondimensional mathematical model consisting of the vorticity Equation (25) and the energy Equation (26). Parameters and variables are made nondimensional using the typical length scales L_x and L_z in the horizontal and vertical directions, a typical velocity U, a plasma reference density ϱ_{α_0}, a reference surface charge density ρ_s, a typical electric permittivity $\langle \epsilon \rangle$, a typical magnetic permeability $\langle \mu \rangle$, a reference plasma thermal expansion κ_α and a reference specific heat capacity at a constant pressure $C_{p,\alpha}$. Denoting the dimensional quantities by asterisks, the corresponding nondimensional quantities are given by:

$$\begin{aligned} &x = \frac{x^*}{L_x}, z = \frac{z^*}{L_z}, t = \frac{t^* U}{L_x}, \Psi_\alpha = \frac{\Psi_\alpha^*}{U L_z}, \varrho_\alpha = \frac{\varrho_\alpha^*}{\varrho_{\alpha_0}}, \bar{\rho}_\alpha = \frac{\bar{\rho}_\alpha^*}{\varrho_{\alpha_0}}, \varrho_{\alpha,el} = \frac{\varrho_{\alpha,el}^*}{\varrho_{\alpha,el_0}}, \eta_e = L_x \eta_e^*, \, \eta_v = L_z \eta_v^*, \\ &g = \frac{L_z g^*}{U^2}, \nu_\alpha = \frac{L_x \nu_\alpha^*}{U L_z^2}, \mathcal{T}_\alpha = \frac{L_x \mathcal{T}_\alpha^*}{U L_z}, B_y = \frac{\varrho_{\alpha,el_0} L_z B_y^*}{U}, E_x = \frac{\varrho_{\alpha,el_0} L_x E_x^*}{U^2} \text{ and } E_z = \frac{\varrho_{\alpha,el_0} L_z E_z^*}{U^2}. \end{aligned} \tag{27}$$

In nondimensional form, Eqs. (25) and (26) respectively become

$$\nabla^2\Psi_{\alpha t} - \Psi_{\alpha z}\nabla^2\Psi_{\alpha x} + \Psi_{\alpha x}\nabla^2\Psi_{\alpha z} + g(\bar{\rho}_\alpha)^{-1}\varrho_{\alpha x} - \nu_\alpha\nabla^4\Psi_\alpha$$
$$-(\varrho_{\alpha,el}B_y)_x\Psi_{\alpha z} + (\varrho_{\alpha,el}B_y)_z\Psi_{\alpha x} + (\varrho_{\alpha,el}E_x)_z - (\varrho_{\alpha,el}E_z)_x = 0. \tag{28}$$

and

$$\varrho_{\alpha t} - \Psi_{\alpha z}\varrho_{\alpha x} + \Psi_{\alpha x}\varrho_{\alpha z} - \mathcal{T}_\alpha\nabla^2\varrho_\alpha = -\nabla\cdot(\mathbf{E}\times\mathbf{H}), \tag{29}$$

where the nondimensional Laplacian and gradient operators are respectively $\nabla^2 = \delta\,\frac{\partial^2}{\partial x^2} + \frac{\partial^2}{\partial z^2}$ and $\nabla = \hat{\mathbf{x}}\sqrt{\delta}\frac{\partial}{\partial x} + \hat{\mathbf{z}}\frac{\partial}{\partial z}$, $\delta = L_z^2/L_x^2$ is the horizontal to vertical aspect ratio.

The vertical length scale L_z has to be of the same order of magnitude as the scale height of the ionosphere H_i in order for the Boussinesq approximation to be valid, while the magnitude of the horizontal length scale L_x is of the same order as that of the horizontal extent of the wave source. This implies $L_z \ll L_x$, and thus the aspect ratio can be considered as a small parameter in the nonedimensional mathematical model. Thus, a small aspect ratio is required in order to simulate long waves ($0 < \delta \ll 1$). Indeed, our mathematical model can be used to simulate ionospheric disturbances with longer horizontal wavelength (MSTIDs and LSTIDs) than atmospheric gravity waves.

2.2. Stochastic Modelling: The Ionosphere as a Weakly-Random Time-Dependent Linear Isotropic Medium

In a weakly-random time-dependent isotropic medium, we express the permittivity $\epsilon(t)$ and the permeability $\mu(t)$ as

$$\epsilon(t) = \langle\epsilon\rangle + \Delta\epsilon(t) \text{ and } \mu(t) = \langle\mu\rangle + \Delta\mu(t), \tag{30}$$

where $\Delta\epsilon(t)$ and $\Delta\mu(t)$ are independent Gaussian random variables with mean zero [32], $\langle\epsilon\rangle$ and $\langle\mu\rangle$ are the averages of the permittivity and permeability respectively, and $\Delta\epsilon(t) \ll \langle\epsilon\rangle$ and $\Delta\mu(t) \ll \langle\mu\rangle$. In that case, the asymptotic approximation $(1+a)^\theta \sim 1+\theta a$ which is valid when $a \ll 1$ can be used to obtain

$$\frac{1}{\epsilon(t)} = \frac{1}{\langle\epsilon\rangle + \Delta\epsilon(t)} \sim \frac{1}{\langle\epsilon\rangle}\left[1 - \frac{\Delta\epsilon(t)}{\langle\epsilon\rangle}\right] \tag{31}$$

and

$$\frac{1}{\mu(t)} = \frac{1}{\langle\mu\rangle + \Delta\mu(t)} \sim \frac{1}{\langle\mu\rangle}\left[1 - \frac{\Delta\mu(t)}{\langle\mu\rangle}\right]. \tag{32}$$

Therefore,

$$\int \frac{1}{\epsilon(\tau)}d\tau \sim \frac{t}{\langle\epsilon\rangle}. \tag{33}$$

Next, substituting Eq. (31) in Eq. (15), we obtain the nondimensional electric field vector

$$\begin{aligned}\mathbf{E}(x,z,t) &= \hat{\mathbf{x}}E_x(x,z,t) + \hat{\mathbf{z}}E_z(x,z,t)\\ &\sim \hat{\mathbf{x}}e^{\sqrt{\delta}\eta_e(z-z_2)}\sin(\eta_e x)\left[1 - \frac{\Delta\epsilon(t)}{\langle\epsilon\rangle}\right] + \hat{\mathbf{z}}e^{\sqrt{\delta}\eta_v(z-z_2)}\cos(\eta_v x)\left[1 - \frac{\Delta\epsilon(t)}{\langle\epsilon\rangle}\right].\end{aligned} \tag{34}$$

Substituting Eq. (32) in Eq. (18) gives the nondimensional magnetic flux density

$$\mathbf{B}(x,z,t) = \hat{\mathbf{y}}B_y \sim -\hat{\mathbf{y}}\,f(t)\left[\eta_e e^{\sqrt{\delta}\eta_e(z-z_2)}\sin(\eta_e x) + \eta_v e^{\sqrt{\delta}\eta_v(z-z_2)}\sin(\eta_v x)\right]t. \tag{35}$$

The magnetic flux density is indeed linear in time. Thus, using Faraday's law of induction, we should obtain a constant electromotive force (voltage), showing that the ionosphere acts as a direct current dynamo [22].

Using (9), we obtain the nondimensional magnetic field vector

$$\mathbf{H}(x,z,t) = \frac{\mathbf{B}(x,z,t)}{\mu(t)} = \hat{\mathbf{y}}H_y \sim -\hat{\mathbf{y}}\,f(t)\,t\left[\eta_e e^{\sqrt{\delta}\eta_e(z-z_2)}\sin(\eta_e x) + \eta_v e^{\sqrt{\delta}\eta_v(z-z_2)}\sin(\eta_v x)\right]\left[1 - \frac{\Delta\mu(t)}{\langle\mu\rangle}\right], \tag{36}$$

and from Eq. (17), we obtain the nondimensional electric charge density

$$\varrho_{\alpha,el}(x,z,t) = f(t)\left[\eta_e e^{\sqrt{\delta}\eta_e(z-z_2)}\cos(\eta_e x) + \eta_v e^{\sqrt{\delta}\eta_v(z-z_2)}\cos(\eta_v x)\right]. \tag{37}$$

The vorticity Equation (28) can thus be rewritten as

$$\begin{aligned}&\nabla^2\Psi_{\alpha_t} - \Psi_{\alpha_z}\nabla^2\Psi_{\alpha_x} + \Psi_{\alpha_x}\nabla^2\Psi_{\alpha_z} + g(\bar{\rho}_\alpha)^{-1}\varrho_{\alpha_x} - \nu_\alpha\nabla^4\Psi_\alpha\\ &-\Gamma_1(x,z,t)\Psi_{\alpha_z} + \Gamma_2(x,z,t)\Psi_{\alpha_x} + \Gamma_3(x,z,t)\left[1 - \frac{\Delta\epsilon(t)}{\langle\epsilon\rangle}\right] = 0,\end{aligned} \tag{38}$$

where $\Gamma_1(x,z,t)$, $\Gamma_2(x,z,t)$ and $\Gamma_3(x,z)$ are given respectively by

$$\begin{aligned}\Gamma_1(x,z,t) =&[\varrho_{\alpha,el}(x,z)B_y(x,z,t)]_x\\ =&-tf(t)\Big\{\sqrt{\delta}\left[\eta_e^3 e^{2\sqrt{\delta}\eta_e(z-z_2)}\cos(2\eta_e x) + \eta_v^3 e^{2\sqrt{\delta}\eta_v(z-z_2)}\cos(2\eta_v x)\right]\\ &+\frac{\eta_e\eta_v}{2}e^{\sqrt{\delta}(\eta_e+\eta_v)(z-z_2)}\left[(1+\delta)(\eta_e+\eta_v)\cos((\eta_e+\eta_v)x)+(1-\delta)(\eta_v-\eta_e)\cos((\eta_v-\eta_e)x)\right]\Big\},\end{aligned} \tag{39}$$

$$\begin{aligned}\Gamma_2(x,z,t) =&[\varrho_{\alpha,el}(x,z)B_y(x,z,t)]_z\\ =&-tf(t)\Big\{\delta\left[\eta_e^3 e^{2\sqrt{\delta}\eta_e(z-z_2)}\sin(2\eta_e x) + \eta_v^3 e^{2\sqrt{\delta}\eta_v(z-z_2)}\sin(2\eta_v x)\right]\\ &+\frac{\sqrt{\delta}\eta_e\eta_v(\eta_e+\eta_v)}{2}e^{\sqrt{\delta}(\eta_e+\eta_v)(z-z_2)}\left[(1+\delta)\sin((\eta_e+\eta_v)x) + (1-\delta)\sin((\eta_v-\eta_e)x)\right]\Big\}\end{aligned} \tag{40}$$

and

$$\begin{aligned}\Gamma_3(x,z,t) =&(\varrho_{\alpha,el}E_x)_z - (\varrho_{\alpha,el}E_z)_x\\ =&\sqrt{\delta}f(t)\left[\eta_e^2 e^{2\sqrt{\delta}\eta_e(z-z_2)}\sin(2\eta_e x) - \eta_v^2 e^{2\sqrt{\delta}\eta_v(z-z_2)}\sin(2\eta_v x)\right]\\ &+\frac{\delta\eta_v(\eta_v+\eta_e)}{2}e^{\sqrt{\delta}(\eta_e+\eta_v)(z-z_2)}[\sin((\eta_v+\eta_e)x) + \sin((\eta_v-\eta_e)x)]\\ &-\frac{\eta_e}{2}e^{\sqrt{\delta}(\eta_e+\eta_v)(z-z_2)}[(\eta_v+\eta_e)\sin((\eta_v+\eta_e)x) + (\eta_e-\eta_v)\sin((\eta_e-\eta_v)x)].\end{aligned} \tag{41}$$

Using the fact that $\Delta\epsilon(t)$ is a random variable with mean zero and $\Delta\epsilon(0) = 0$, $\Delta\epsilon(t)/\langle\epsilon\rangle$ can be written as $\sigma_E\dot{W}_E(t)$ in Eq. (38) where $\dot{W}_E(t)$ is a Wiener process, and σ_E is a small constant [21, 22]. Hence, the vorticity Equation (38) becomes

$$\begin{aligned}&\nabla^2\Psi_{\alpha_t} - \Psi_{\alpha_z}\nabla^2\Psi_{\alpha_x} + \Psi_{\alpha_x}\nabla^2\Psi_{\alpha_z} + g(\bar{\rho}_\alpha)^{-1}\varrho_{\alpha_x} - \nu_\alpha\nabla^4\Psi_\alpha\\ &-\Gamma_1(x,z,t)\Psi_{\alpha_z} + \Gamma_2(x,z,t)\Psi_{\alpha_x} = -\Gamma_3(x,z,t) + \sigma_E\Gamma_3(x,z,t)\dot{W}_E(t),\end{aligned} \tag{42}$$

where the last two terms on the left hand side of Eq. (42) represent the magnetohydrodynamic effects, while the terms on right hand side of Eq. (42) represent the electrohydrodynamic effects.

Before reformulating the energy Equation (29), let us recall the conservation of the electromagnetic energy (or Poynting Theorem) [4]

$$-\nabla\cdot(\mathbf{E}\times\mathbf{H}) = \frac{\partial E_{EM}}{\partial t} + \mathbf{E}\cdot\mathbf{J} = \left[\mathbf{E}\cdot\frac{\partial\mathbf{D}}{\partial t} + \mathbf{H}\cdot\frac{\partial\mathbf{B}}{\partial t}\right] + \mathbf{E}\cdot\mathbf{J}, \tag{43}$$

where $\frac{\partial E_{EM}}{\partial t} = \mathbf{E}\cdot\frac{\partial\mathbf{D}}{\partial t} + \mathbf{H}\cdot\frac{\partial\mathbf{B}}{\partial t}$ is the electromagnetic energy density rate; $\mathbf{E}\cdot\frac{\partial\mathbf{D}}{\partial t}$ is the electric energy density rate; $\mathbf{H}\cdot\frac{\partial\mathbf{B}}{\partial t}$ is the magnetic energy density rate; and $\mathbf{E}\cdot\mathbf{J}$ is the energy (in form of heat or Joule heating) dissipating rate density. Our study focuses on disturbances generated via Lorentz force, the Joule heating $\mathbf{E}\cdot\mathbf{J}$ will therefore be omitted in our mathematical model.

We note that the electric energy density rate is zero, $\mathbf{E}\cdot\frac{\partial\mathbf{D}}{\partial t} = 0$ since, according to Eq. (16), $\frac{\partial\mathbf{D}}{\partial t} = 0$. In that case, in the numerical modelling of electrohydrodynamic disturbances (EHD), the energy Equation (29) reduces to

$$\varrho_{\alpha_t} - \Psi_{\alpha_z}\varrho_{\alpha_x} + \Psi_{\alpha_x}\varrho_{\alpha_z} - \mathcal{T}_\alpha\nabla^2\varrho_\alpha = 0, \tag{44}$$

which is the same as the energy equation associated to internal gravity waves in the neutral (lower) atmosphere [29]. In the numerical modelling of magnetohydrodynamic (MHD) disturbances, on the other hand, the divergence of the Poynting vector $\nabla \cdot (\mathbf{E} \times \mathbf{H})$ (or the electromagnetic energy rate per unit of volume) is thus given by

$$\begin{aligned}\nabla \cdot (\mathbf{E}\times\mathbf{H}) &= -\frac{\partial E_{EM}}{\partial t} = -\mathbf{H}\cdot\frac{\partial \mathbf{B}}{\partial t} \\ &\sim -\frac{tf(t)}{2}\Bigg\{\delta\eta_e^2 e^{2\sqrt{\delta}\eta_e(z-z_2)}\left[1-\cos(2\eta_e x)\right] + \eta_v^2 e^{2\sqrt{\delta}\eta_v(z-z_2)}\left[1-\cos(2\eta_v x)\right] \\ &\quad + 2\sqrt{\delta}\eta_v\eta_e e^{\sqrt{\delta}(\eta_v+\eta_e)(z-z_2)}\left[\cos((\eta_v-\eta_e)x) - \cos((\eta_v+\eta_e)x)\right]\Bigg\}\left[1-\frac{\Delta\epsilon(t)}{\langle\epsilon\rangle}\right]\left[1-\frac{\Delta\mu(t)}{\langle\mu\rangle}\right].\end{aligned} \tag{45}$$

Next, substituting Eq. (45) into the energy Equation (29) and neglecting the term of order $O\left[(\Delta\epsilon(t)/\langle\epsilon\rangle)\,(\Delta\mu(t)/\langle\mu\rangle)\right]$, the energy equation can thus be written as

$$\varrho_{\alpha_t} - \Psi_{\alpha_z}\varrho_{\alpha_x} + \Psi_{\alpha_x}\varrho_{\alpha_z} - \kappa_\alpha\nabla^2\varrho_\alpha = \Gamma_4(x,z,t)\left[1-\frac{\Delta\epsilon(t)}{\langle\epsilon\rangle}-\frac{\Delta\mu(t)}{\langle\mu\rangle}\right], \tag{46}$$

where

$$\begin{aligned}\Gamma_4(x,z,t) \sim \frac{tf(t)}{2}\Bigg\{&\delta\eta_e^2 e^{2\sqrt{\delta}\eta_e(z-z_2)}\left[1-\cos(2\eta_e x)\right] + \eta_v^2 e^{2\sqrt{\delta}\eta_v(z-z_2)}\left[1-\cos(2\eta_v x)\right] \\ &+ 2\sqrt{\delta}\eta_v\eta_e e^{\sqrt{\delta}(\eta_v+\eta_e)(z-z_2)}\left[\cos((\eta_v-\eta_e)x) - \cos((\eta_v+\eta_e)x)\right]\Bigg\}.\end{aligned} \tag{47}$$

We write $\Delta\mu(t)/\langle\mu\rangle$ as $\sigma_H\dot{W}_H(t)$ where $\dot{W}_H(t)$ is a Wiener process, and σ_H is a small constant. This gives the stochastic energy equation

$$\varrho_{\alpha_t} - \Psi_{\alpha_z}\varrho_{\alpha_x} + \Psi_{\alpha_x}\varrho_{\alpha_z} - \mathcal{T}_\alpha\nabla^2\varrho_\alpha = \Gamma_4(x,z,t) - \Gamma_4(x,z,t)[\sigma_E\dot{W}_E(t) + \sigma_H\dot{W}_H(t)]. \tag{48}$$

3. NUMERICAL IMPLEMENTATION

In this section, we describe our numerical model. It is obtained using a procedure similar to that in [20]. The numerical model consists of the nondimensional vorticity Equation (42), and the nondimensional energy Equation (48), where each dependent variable is defined as a sum of an initial mean part and a time-dependent perturbation part (or wave).

We write

$$\Psi_\alpha(x,z,t) = \bar{\psi}_\alpha(z) + \varepsilon\psi_\alpha(x,z,t) \;\text{ and }\; \varrho_\alpha(x,z,t) = \bar{\rho}_\alpha(z) + \varepsilon\rho_\alpha(x,z,t). \tag{49}$$

where $\varepsilon = \frac{L_z U}{\varphi} \ll 1$ and φ is the dimensional amplitude of the wave at the source, and as before, L_z is the vertical length scale while U is a typical velocity scale. Substituting Eq. (49) into Eqs. (42) and (48), we obtain

$$\begin{aligned}&\zeta_{\alpha_t} + \bar{u}_\alpha\zeta_{\alpha_x} - \bar{u}_\alpha^{''}\psi_{\alpha_x} + \varepsilon(\psi_{\alpha_x}\zeta_{\alpha_z} - \psi_{\alpha_z}\zeta_{\alpha_x}) + g(\bar{\rho}_\alpha)^{-1}\varrho_{\alpha_x} - \nu_\alpha\nabla^2\zeta_\alpha \\ &-\Gamma_1(x,z,t)(-\varepsilon^{-1}\bar{u}_\alpha + \psi_{\alpha_z}) + \Gamma_2(x,z,t)\psi_{\alpha_x} = -\Gamma_3(x,z,t) + \sigma_E\Gamma_3(x,z,t)\dot{W}_E(t),\end{aligned} \tag{50}$$

$$\zeta_\alpha = \nabla^2\psi_\alpha \tag{51}$$

and

$$\rho_{\alpha_t} + \bar{u}_\alpha\rho_{\alpha_x} + \bar{\rho}_\alpha^{'}\psi_{\alpha_x} + \varepsilon(\psi_{\alpha_x}\rho_{\alpha_z} - \psi_{\alpha_z}\rho_{\alpha_x}) - \mathcal{T}_\alpha\nabla^2\rho_\alpha = \Gamma_4(x,z,t) - \Gamma_4(x,z,t)[\sigma_E\dot{W}_E(t) + \sigma_H\dot{W}_H(t)], \tag{52}$$

where the superscript prime indicates a derivative with respect to z.

The small parameter ε characterizes the nonlinearities due to wave-wave interactions. In the present study, we examine the nonlinear interactions between the electromagnetic field and the waves and

consider a configuration in which the parameter ε is small enough that the nonlinear terms (representing the nonlinear wave-wave interactions) that multiplies ε can be neglected.

We solve Eqs. (50)–(52) on a rectangular domain in the vertical plane defined by $0 \leq x \leq 2\pi$ and $z_1 \leq z \leq z_2$ subject to the initial conditions

$$\psi_\alpha(x, z, 0) = \zeta_\alpha(x, z, 0) = \rho_\alpha(x, z, 0) = 0 \tag{53}$$

and the boundary conditions,

$$\psi_\alpha(x, z_1, t) = \zeta_\alpha(x, z_1, t) = \rho_\alpha(x, z_1, t) = 0, \tag{54}$$

and

$$\psi_\alpha(x, z_2, t) = \zeta_\alpha(x, z_2, t) = \rho_\alpha(x, z_2, t) = 0. \tag{55}$$

In the simulations, we numerically solve Eq. (50)–(55) using a WCE-based numerical method as described in [20, 21]. This method effectively transforms a stochastic initial boundary value problem into a deterministic one by separating the random effects from the deterministic effects. The deterministic problem is then solved using an appropriate classical numerical method. Here, we use the predictor-corrector method used in [21, 23], which uses the second-order Adams-Bashforth as a predictor scheme and the second-order Adams-Moulton scheme as a corrector scheme. This technique is stable and relatively large time and large space increments can be used while the magnitude of errors remains small [21, 23].

We numerically simulate the electrohydrodynamic disturbances (EHD) generated by the effects due the electric field and the magnetohydrodynamic disturbances (MHD) generated by the effects due to the magnetic field. In the simulations of EHD interactions, the terms representing the effects due to the magnetic fields are set to zero in the plasma vorticity Equation (50) and in the energy Equation (52) ($\Gamma_1 = \Gamma_2 = \Gamma_4 = 0$), while the terms representing the electric field effects are nonzero ($\Gamma_3 \neq 0$). In the simulations of MHD interactions, the terms representing the effects due to the magnetic field are nonzero in the plasma vorticity Equation (50) and in the energy Equation (52) ($\Gamma_1 \neq 0$, $\Gamma_2 \neq 0$ and $\Gamma_4 \neq 0$), while the terms representing the electric field effects are neglected ($\Gamma_3 = 0$).

4. THE RESULTS OF THE NUMERICAL SIMULATIONS

Simulations are performed over the nondimensional time interval from $t = 0$ to $t = 20$ on a rectangular domain given by $0 < x < 2\pi$ and $40 < z < 80$. Following [21], we can deduce that the numerical errors will be order 10^{-2} at $t = 20$. In the numerical simulations, the nondimensional acceleration due to gravity is set to $g = 9.8$ and the buoyancy frequency to $N = 1$ so that using Eq. (24) gives the ionospheric height scale $H_i = 9.8$. The kinematic viscosity is set to $\nu_\alpha = 10^{-6}$. The mean flow velocity is $\bar{u}_\alpha = 4$. We first perform numerical simulations with the aspect ratio $\delta = 0.2$ and then with $\delta = 0.1$ to simulate long waves. The choice of these parameters will be clear once our results are dimensionalized (see Section 4.3).

We also ensure that $\Delta\epsilon(t)/\langle\epsilon\rangle = \delta_E W_E(t)$ and $\Delta\mu(t)/\langle\mu\rangle = \delta_H W_H(t)$ are indeed smaller than 1 ($\Delta\epsilon(t)/\langle\epsilon\rangle \ll 1$ and $\Delta\mu(t)/\langle\mu\rangle \ll 1$) for all t. To do so, we generate the random vectors of W_E values and W_H values, and respectively identify their maximum values over the time interval and thus set $\delta_E = 0.01/|\max\{W_E\}|$ and $\delta_H = 0.01/|\max\{W_H\}|$, see for example [22]. Therefore, the amplitude of the random fluctuations is small relative to the deterministic part (the mean), and hence solutions are almost deterministic.

4.1. EHD: Electrohydrodynamic Effects and Generation of Small Scale TIDs ($\Gamma_1 = \Gamma_2 = \Gamma_4 = 0$, $\Gamma_3 \neq 0$)

In the numerical simulations of EHD disturbances, $\Gamma_1 = \Gamma_2 = 0$ in Eq. (50) and $\Gamma_4 = 0$ in Eq. (52). We set $\eta_e = 2\eta$ and $\eta_v = \eta$ so that

$$\begin{aligned}\Gamma_3(x, z, t) \;=\; & \eta^2 f(t)\Big\{0.45e^{0.9\eta(z-z_2)}\sin(2\eta x) - 1.8e^{1.8\eta(z-z_2)}\sin(4\eta x) \\ & -e^{1.35\eta(z-z_2)}[0.15\sin(3\eta x) + 0.85\sin(\eta x)]\Big\},\end{aligned} \tag{56}$$

and, according to (56), the electric field generates the horizontal wavenumbers $\eta, 2\eta, 3\eta$ and 4η. We also set $\langle\epsilon\rangle = -1.5$ as in [22], and $\eta = 1$. In the switch-off function $f(t)$, $t_0 = 5$.

We can approximate the nondimensional mean horizontal wavenumber of the EHD perturbations at early time as $\langle k_x\rangle = \sum_i |k_i||\langle\hat{\psi}_{\alpha_i}\rangle|/\sum_i |\langle\hat{\psi}_{\alpha_i}\rangle|$, where as before, $|\langle\hat{\psi}_{\alpha_i}\rangle|$ is an absolute value of the weight corresponding to the wavenumber k_i on Figure 4(a), and thus obtain $\langle k_x\rangle \approx 1.63$ so that the nondimensional horizontal wavelength at early time is approximately $\langle\lambda_x\rangle = 2\pi/\langle k_x\rangle = 1.23\pi$. According to Figure 4(b), on the other hand, the nondimensional horizontal wavenumber of the EHD disturbances at a later time, $t \geq 10$, is $\langle k_x\rangle \approx 1$, and so $\langle\lambda_x\rangle = 2\pi/\langle k_x\rangle = 2\pi$ as observed in Figure 1(b). This demonstrates that EHD disturbances have almost doubled their wavelength at $t = 10$, which then remained constant after $t = 10$ as in the case of linear atmospheric GWs [29].

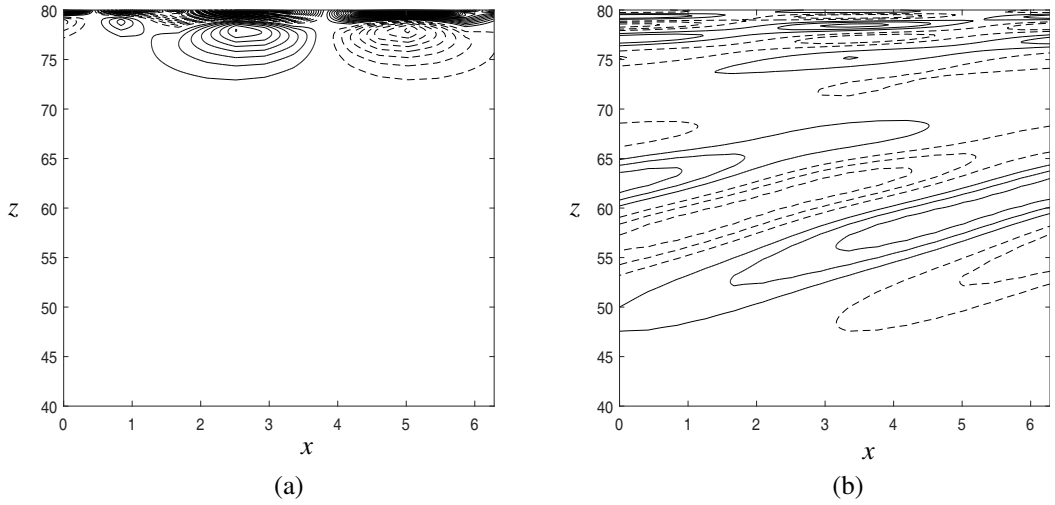

Figure 1. EHD disturbances: contour plots of the mean horizontal (component) velocity perturbation $\langle -\psi_{\alpha_z}(x, z, t)\rangle$, (a) at $t = 1$ and (b) at $t = 20$. The overall wavenumber of the perturbations in (a) is greater than that of the perturbations in (b). The vertical to horizontal aspect ratio is $\delta = 0.2$.

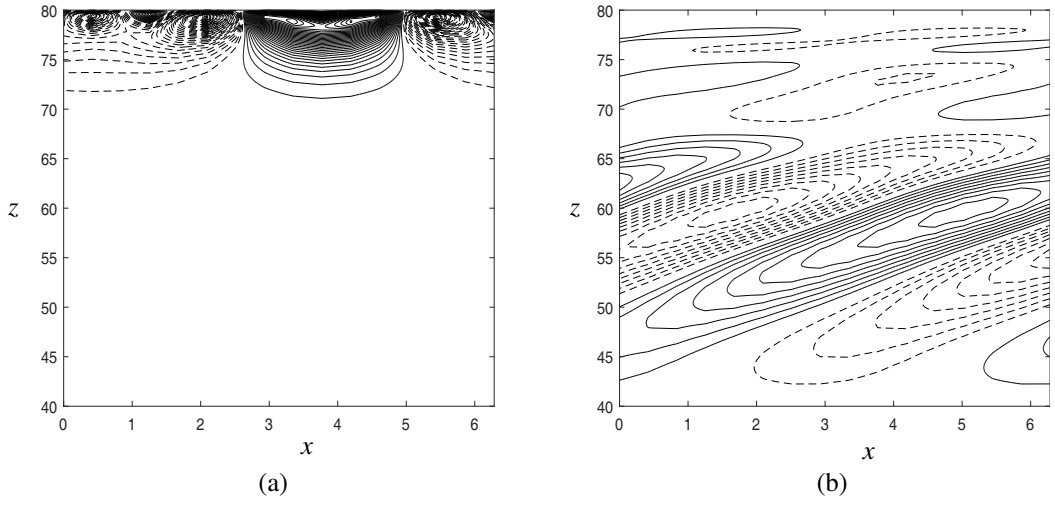

Figure 2. EHD disturbances: contour plots of the mean vertical (component) velocity perturbations $\langle \psi_{\alpha_x}(x, z, t)\rangle$, (a) at $t = 1$ and (b) at $t = 20$. The overall wavenumber of the perturbations in (a) is greater than that of the perturbations in (b). The horizontal to vertical aspect ratio is $\delta = 0.2$.

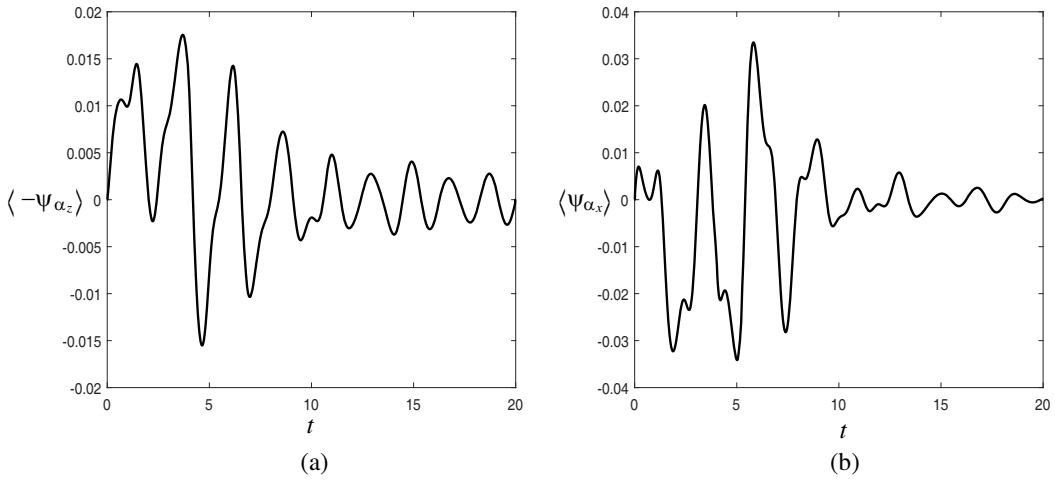

Figure 3. EHD disturbances: the mean amplitude of the wave perturbations as a function of time t in the center of our rectagular domain. In (a) the mean amplitude of the perturbations of the horizontal component of the velocity $\langle -\psi_{\alpha_z}(x,z,t)\rangle$, and (b) the mean amplitude of the perturbations of the vertical component of the velocity $\langle \psi_{\alpha_x}(x,z,t)\rangle$. The horizontal to vertical aspect ratio is $\delta = 0.2$.

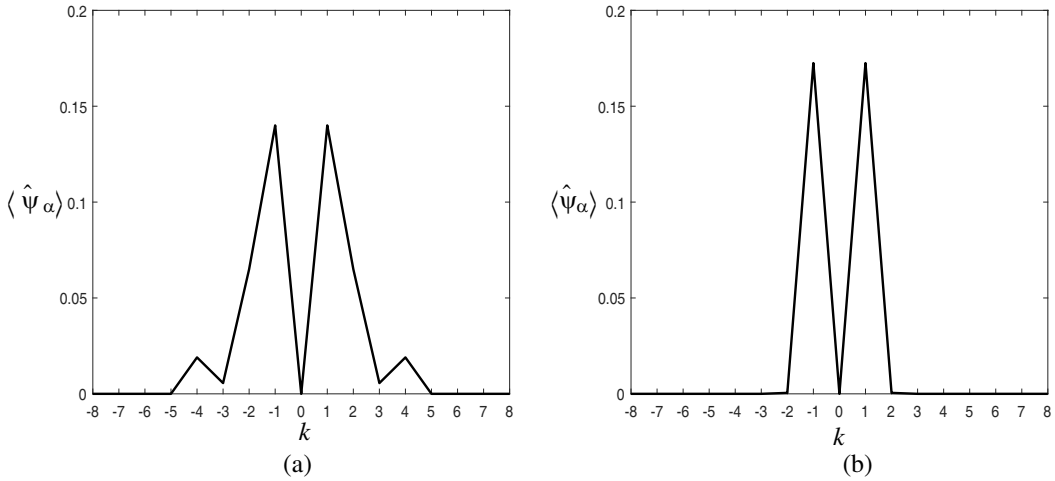

Figure 4. EHD disturbances: Fourier spectrum of the mean amplitude of the wave streamfunction $\langle \hat{\psi}_\alpha(k,z,t)\rangle$ as a function of the wavenumber k at height $z = 60$, and at the time, (a) $t = 1$ and (b) $t = 20$. The horizontal to vertical aspect ratio is $\delta = 0.2$.

4.2. MHD: Magnetohydrodynamic Effects and Generation of Medium and Large Scale TIDs ($\Gamma_1 \neq 0$, $\Gamma_2 \neq 0$, $\Gamma_4 \neq 0$ $\Gamma_3 = 0$)

In the numerical simulations of MHD waves, $\Gamma_3 = 0$, while $\Gamma_1 \neq 0$ and $\Gamma_2 \neq 0$ in (48). We also consider that $\eta_e = 2\eta$ and $\eta_v = \eta$ as in Section 4.1. This gives

$$\begin{aligned}\Gamma_1(x,z,t) \;=\; & -\eta^3 t\Big\{3.6\, e^{1.8\eta(z-z_2)}\cos(4\eta x) + 0.45\, e^{0.9\eta(z-z_2)}\cos(2\eta x) \\ & + e^{1.35\eta(z-z_2)}\left[3.6\cos(3\eta x) - 0.8\cos(\eta x)\right]\Big\}, \end{aligned} \tag{57}$$

$$\begin{aligned}\Gamma_2(x,z,t) \;=\; & -\eta^3 t\Big\{1.6\, e^{1.8\eta(z-z_2)}\sin(4\eta x) + 0.2\, e^{0.9\eta(z-z_2)}\sin(2\eta x) \\ & + 1.35\, e^{1.35\eta(z-z_2)}\left[1.2\sin(3\eta x) - 0.8\sin(\eta x)\right]\Big\} \end{aligned} \tag{58}$$

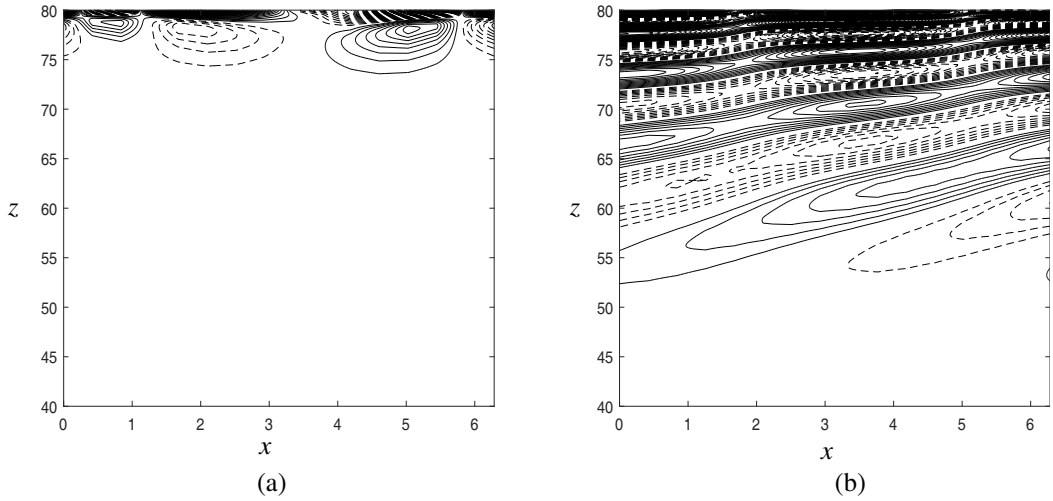

Figure 5. MHD disturbances: contour plots of the mean horizontal (component) velocity perturbation $\langle -\psi_{\alpha_z}(x,z,t)\rangle$, (a) at $t=1$ and (b) at $t=20$. The overall wavenumber of the perturbations in (a) is greater than that of the perturbations in (b) as in Figure 1. The horizontal to vertical aspect ratio is $\delta = 0.2$.

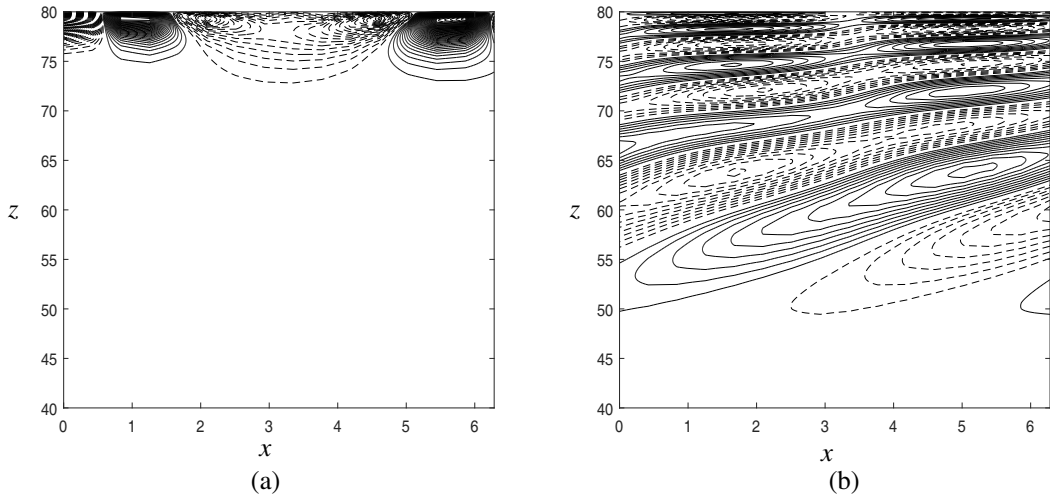

Figure 6. MHD disturbances: contour plots of the mean vertical (component) velocity perturbation $\langle \psi_{\alpha_x}(x,z,t)\rangle$, (a) at $t=1$ and (b) at $t=20$. The overall wavenumber of the perturbations in (a) is greater than that of the perturbations in (b) as in Figure 2. The horizontal to vertical aspect ratio is $\delta = 0.2$.

and

$$\Gamma_4(x,z,t) \;=\; \eta^2 f(t)\, t \Big\{ 0.4 e^{1.8\eta(z-z_2)}[1-\cos(4\eta x)] + 0.5\, e^{0.9\eta(z-z_2)}[1-\cos(2\eta x)] \\ +0.9\, e^{1.35\eta(z-z_2)}\,[\cos(\eta x)-\cos(3\eta x)]\Big\}. \tag{59}$$

In contrast to EHD waves, we expect that MHD waves develop the zero wavenumber harmonic corresponding to the mean flow evolution as the result of nonlinear interactions between waves and the ionosphere via the Lorentz force as seen in Figure 8 (the nonlinear terms involving Γ_1 and Γ_2). This shows that there is a transfer of momentum flux to the mean flow.

The nondimensional mean horizontal wavenumber of MHD perturbations can be approximated as $\langle k_x\rangle = \sum_i |k_i||\langle\hat{\psi}_{\alpha_i}\rangle|/\sum_i |\langle\hat{\psi}_{\alpha_i}\rangle|$, where as before, $|\langle\hat{\psi}_{\alpha_i}\rangle|$ is the absolute value of the weight

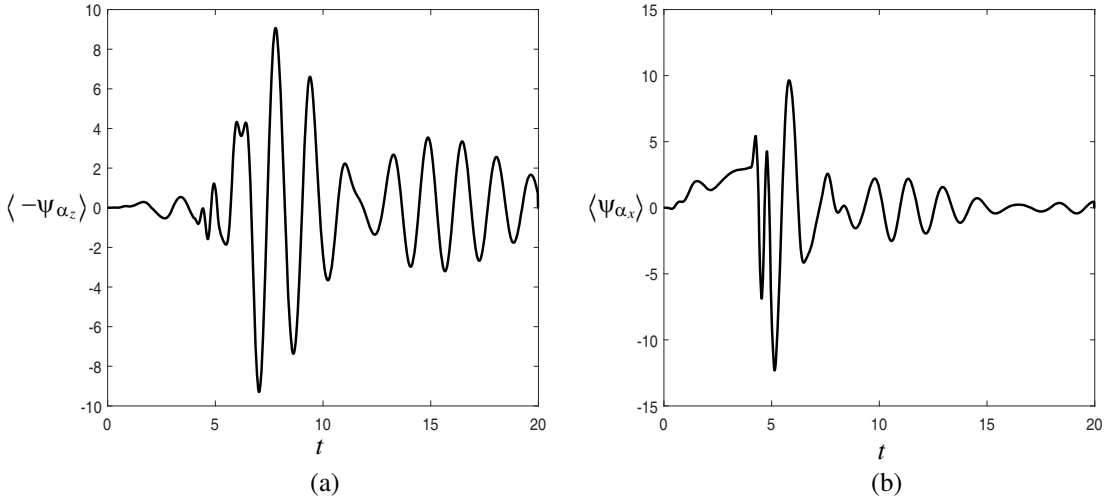

Figure 7. MHD disturbances: the mean amplitude of wave perturbations as a function of time t near the upper boundary of our rectagular domain. In (a) the mean amplitude of the perturbations of the horizonal component of the velocity $\langle -\psi_{\alpha_z}(x,z,t)\rangle$, and (b) the mean amplitude of the perturbations of the vertical component of the velocity $\langle \psi_{\alpha_x}(x,z,t)\rangle$. The horizontal to vertical aspect ratio is $\delta = 0.2$.

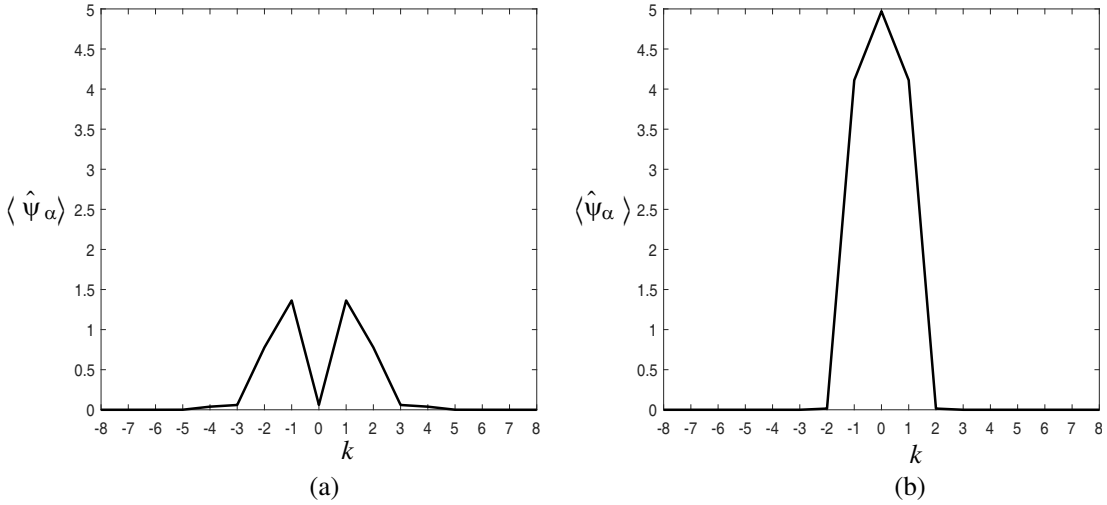

Figure 8. MHD disturbances: Fourier spectrum of the mean amplitude of the wave streamfunction $\langle\hat{\psi}_\alpha(k,z,t)\rangle$ as a function of the wavenumber k at height $z = 60$, and at the time, (a) $t = 1$ and (b) $t = 20$. The horizontal to vertical aspect ratio is $\delta = 0.2$.

corresponding to the wavenumber k_i. Using the data that we have used to obtain Figures 8(a) and 8(b), we thus obtain $\langle k_x\rangle \approx 1.41$ at early time, while $\langle k_x\rangle \approx 0.47$ at a later time. This gives the overall wavelength $\langle\lambda_x\rangle \approx 2\pi/\langle k_x\rangle \approx 1.41\pi$ and $\langle\lambda_x\rangle \approx 2\pi/\langle k_x\rangle = 4.25\pi$ at early and later time respectively as may be observed in Figures 5 and 6 showing that at $t = 20$, MHD disturbances have tripled their wavelengths.

Our results show that MHD disturbances have longer wavelengths than EHD disturbances. Further, when comparing Figure 7 against Figure 3, the amplitude of EHD disturbances is smaller than that of MHD showing that the effects due to the electric field are weaker compared to those due to the magnetic field. Therefore, numerical simulations of the combined electric and magnetic effects should not produce any new result.

4.2.1. Configuration Where the Horizontal to Vertical Aspect Ratio $\delta = 0.1$

In addition, we also performed numerical simulations, where the horizontal to vertical aspect ratio $\delta = 0.1$, in order to simulate longer waves than when the aspect ratio $\delta = 0.2$. We obtained that EHD disturbances have the horizontal nondimensional $\langle\lambda_x\rangle \approx 1.44\pi$ rather than $\langle\lambda_x\rangle \approx 1.23\pi$ as obtained in the configuration where $\delta = 0.2$. The nondimesional wavelength did increase and reached the nondimensional value $\langle\lambda_x\rangle \approx 2\pi$ at a later time and then remained constant as in the linear atmospheric gravity wave case as before.

We have, as well, simulated MHD perturbations in a configuration where $\delta = 0.1$. We found that MHD disturbances have the nondimensional horizontal wavelength $\langle\lambda_x\rangle \approx 1.50\pi$ at early time and reached $\langle\lambda_x\rangle \approx 5.62\pi$ at a later time, showing that the horizontal wavelength are longer than in the configuration where $\delta = 0.2$. The nondimensional horizontal wavelength of the MHD disturbances have quadrupled at $t = 20$ rather than triple as in the configuration where $\delta = 0.2$. In the next section, we examine the corresponding dimensional quantities.

4.3. Dimensional Analysis

We consider that the α-species in the ionospheric F region are predominantly oxygen ions, and their average temperature is around $T_\alpha \approx 1100\,\mathrm{K}$ [33]. Then the ionospheric scale height is approximately $H_i^* \approx k/(m_\alpha g)T_\alpha = 29.2\,\mathrm{km}$. The value of the nondimensional height scale in the numerical simulations is $H_i = 9.8$, and so, the vertical length scale $L_z = H_i^*/H_i = 3.0\,\mathrm{km}$. Thus the wave source, or the upper boundary of our rectangular domain, is in the ionospheric F region at 238 km above the planet Earth, while the lower boundary is in the ionospheric F region at 119 km above the planet Earth.

4.3.1. Configuration Where the Horizontal to Vertical Aspect Ratio $\delta = 0.2$: Small Scale Travelling Ionospheric Disturbances (SSTDIs)

In the configuration where the horizontal to vertical aspect ratio $\delta = 0.2$, the horizontal length scale $L_x = L_z/\sqrt{\delta} = 6.7\,\mathrm{km}$. This implies that at early time the EHD disturbance wavelength is $\langle\lambda_x^*\rangle = \langle\lambda_x\rangle \cdot L_x \approx 1.23\pi \cdot L_x = 26.0\,\mathrm{km}$, while at a later time, $\langle\lambda_x^*\rangle = \langle\lambda_x\rangle \cdot L_x \approx 2\pi \cdot L_x = 42.1\,\mathrm{km}$. Therefore, $1.50 \cdot 10^4\,\mathrm{m}^{-1} \le \langle k_x^*\rangle \le 2.42 \cdot 10^{-4}\,\mathrm{m}^{-1}$. In the numerical simulations, the acceleration due gravity $g = 9.8$, so its dimensional scale is $g^*/g = (9.8/9.8)\,\mathrm{m\ sec}^{-2} = 1\,\mathrm{m\ sec}^{-2}$. This implies that the velocity scale $U = \sqrt{L_z\, g^*/g} = 54.8\,\mathrm{m\ sec}^{-1}$, and so the dimensional mean flow velocity $\bar{u}_\alpha^* = \bar{u}_\alpha U = 4 \cdot 54.8\,\mathrm{m\ sec}^{-1} = 219.2\,\mathrm{m\ sec}^{-1}$.

Using Eq. (24), the buoyancy frequency is approximately $N_i = \sqrt{g^*/H_i^*} = 0.02\,\mathrm{sec}^{-1}$. Therefore, following the linear stability theory of atmospheric GWs [29], it can readily be shown that if the perturbations generated as a result of the buoyancy effects are travelling (or are waves), then their mean vertical wavenumber $\langle m^*\rangle$ should satisfy $\langle m^*\rangle^2 = {N_i^*}^2/{\bar{u}_\alpha^*}^2 - \langle k^*\rangle^2 > 0$. So, their cut-off horizontal wavenumber has to satisfy $\langle k_{xc}^*\rangle < N_i^*/\bar{u}_\alpha^* = (0.02/219.2)\,\mathrm{m}^{-1} = 0.91 \cdot 10^{-4}\,\mathrm{m}^{-1}$. Therefore, EHD perturbations simulated in this study are not travelling since their mean horizontal wavenumber is greater than the cut off horizontal wavenumber, $\langle k_x^*\rangle > \langle k_{x_c}^*\rangle = 0.91 \cdot 10^{-4}\,\mathrm{m}^{-1}$. This implies that the wavelength of travelling disturbances have to be longer than $\langle\lambda_{x_c^*}\rangle = 2\pi/\langle k_{xc}^*\rangle = 69.0\,\mathrm{km}$.

The time scale is L_x/U, and so this suggests that EHD disturbances took the time $t^* = (L_x/U)t \approx 41\,\mathrm{min}$ to double their wavelength, while MHD disturbances have tripled their wavelength.

MHD perturbations simulated in this study have a mean horizontal wavenumber $\langle k_x^*\rangle \approx 2.10 \cdot 10^{-4}\,\mathrm{m}^{-1}$ at early time, while at a later time, their mean horizontal wavenumber is $\langle k_x^*\rangle \approx 0.70 \cdot 10^{-4}\,\mathrm{m}^{-1}$. In this case at a later time, $\langle\lambda_x^*\rangle \approx 89.6\,\mathrm{km}$, showing that our simulated perturbations are small scale disturbances. At a certain time, the wavenumber of the MHD perturbations became small than the cut-off wavenumber, and as a result, MHD perturbations became travelling ionospheric disturbances (SSTIDs). This is in agreement with observations that have shown that smaller spatial and shorter temporal scale disturbances exist in the ionosphere, and that not all disturbances seen are in fact travelling, see for example Harris et al. [9].

4.3.2. Configuration with the Horizontal to Vertical Aspect Ratio $\delta = 0.1$: Medium Scale Travelling Ionospheric Disturbances (MSTIDs)

The goal here is to show that magnetohydrodynamic effects are mainly responsible for medium scale travelling ionospheric disturbances (MSTIDs). Under similar conditions (same pressure and temperature), we can simulate MSTIDs. To do so, we set the horizontal to vertical aspect ratio $\delta = 0.1$. In that case, the horizontal length scale $L_x = L_z/\sqrt{\delta} = 9.5\,\text{km}$. Therefore, at early time, EHD disturbances have an overall wavelength $\langle\lambda_x^*\rangle \approx 42.9\,\text{km}$, while at a later time, $\langle\lambda_x^*\rangle \approx 59.6\,\text{km}$. So, $1.05 \cdot 10^4\,\text{m}^{-1} \leq \langle k_x^*\rangle \leq 1.46 \cdot 10^{-4}\,\text{m}^{-1}$. The velocity scale $U = \sqrt{L_z\, g^*/g} = 97.5\,\text{m sec}^{-1}$, and so the dimensional mean flow velocity $\bar{u}_\alpha^* = \bar{u}_\alpha\, U = 390.0\,\text{m sec}^{-1}$.

The buoyancy frequency, as before, is approximately $N_i = \sqrt{g^*/H_i^*} = 0.02\,\text{sec}^{-1}$. In that case, the cut-off mean horizontal wavenumber for travelling disturbances is $\langle k_{xc}^*\rangle = N_i^*/\bar{u}_\alpha^* = (0.02/390)\,\text{m}^{-1} = 0.5 \cdot 10^{-4}\,\text{m}^{-1}$ corresponding to the cut-off mean horizontal wavelength $\langle\lambda_x^*\rangle = 122.5\,\text{km}$, showing that travelling ionospheric disturbances, in this case, should be MSTIDs, see for example [27, 31]. However, EHD disturbances are small scale disturbances and are non-travelling [9] because their overall wavenumber is greater than the cut-off wavenumber k_{xc}^*.

MHD perturbations, on the other hand, have the dimensional mean horizontal wavelength $\langle\lambda_x^*\rangle = \langle\lambda_x\rangle \cdot L_x \approx 44.8\,\text{km}$ at early time, and $\langle\lambda_x^*\rangle = \langle\lambda_x\rangle \cdot L_x \approx 167.7\,\text{km}$ at later time. This demonstrates our simulated travelling ionospheric disturbances are MSTIDs travelling at the speed $\bar{u}_\alpha^* = 390.0\,\text{m sec}^{-1}$, see for example [27, 31]. Therefore, magnetohydrodynamic effects are responsible for travelling ionospheric disturbances of auroral origin.

The time scale is L_x/U, this suggests that MHD disturbances took the time $t^* = (L_x/U)t \approx 32\,\text{min}$ to quadruple their wavelength.

5. GENERAL DISCUSSION AND CONCLUSIONS

In magnetohydrodynamic (MHD) modeling, the ideal magnetohydrodynamic assumption is commonly used [8, 15]. The substitution $\mathbf{E} = -\mathbf{u} \times \mathbf{B}$ is used for the electric field $\mathbf{E}$ in Maxwell's equations and the energy equations [8, 15]. However, this implies that $\mathbf{E} + \mathbf{u} \times \mathbf{B} = 0$ in the momentum Equation (1). Hence, the momentum equation is reduced to Navier-Stokes equation. As a result of the ideal magnetohydrodynamic assumption, there is no magnetohydrodynamic problem to solve.

The electric field $\mathbf{E}$ is often neglected while the term $\mathbf{u} \times \mathbf{B}$ is kept in the momentum equation in order to avoid this. However, this is in contradiction with the substitution $\mathbf{E} = -\mathbf{u} \times \mathbf{B}$ in Maxwell's and energy equations. Hence, there are inconsistencies in these simplifications. The equations based on these simplifications are what are generally called MHD equations.

To avoid the inconsistencies in the standard MHD formulation, we considered the ionosphere as an isotropic medium with weakly-random fluctuations in time as in [22]. Following [22], we obtained the expressions for $\mathbf{E}$ and $\mathbf{B}$ for a configuration corresponding to an electric dynamo which we substituted in the momentum Equation (2) and energy Equation (3). We then proceeded as in [20], wrote the later equations in streamfunction-vorticity formulation and solved the resulting equations in a configuration where the buoyancy and electrodynamic effects play the main role to generate ionospheric disturbances as has been suggested by [11, 13].

We carried out numerical simulations (see procedure in [20, 21]) and separately investigated the electrohdrodynamic (EHD) and magnetohydrodynamic (MHD) effects. A simple two-dimensional mathematical model for internal gravity waves propagating in the lower atmosphere [29] consisting of a rectangular domain in a plane perpendicular to the surface of the earth with Cartesian coordinates has been used and allowed us to obtain some of the characteristics of the ionospheric disturbances, e.g., wavenumber or wavelength and speed.

Our results suggest that EHD perturbations are small scale non-travelling ionspheric disturbances with an average horizontal wavelength shorter than 100 km. Non-travelling small scale ionospheric disturbances are often observed in the upper atmosphere (see for example [9]), and thus, our study suggests that they are mainly generated by electrohydrodynamic (EHD) effects.

As a result of the magnetohydrodynamic (MHD) effects, we were able to simulate small scale travelling ionspheric disturbances (SSTIDs) with an average wavelength of order 100 km propagating

with a speed of 219 m $\sec^{-1}$, and medium scale treavelling disturbances (MSTIDs) with an average wavelength of order 170 km propagating at a speed of 390 m $\sec^{-1}$ as may be observed in the ionosphere, see for example [9, 27, 31].

Our simulation results have shown that the overall wavelength of the MHD disturbances quadrupled in about a half an hour (30 min) as a result of nonlinear interactions between waves and the ionosphere via the Lorentz force. We should expect that their wavelength will further elongate if simulations are continued over a prolonged period of time so that we obtain large scale travelling ionospheric disturbances (LSTIDs) [7, 27, 31]. However, we have stopped our numerical simulations early to avoid wave reflections at the out flow (lower) boundary which would significantly affect our simulation results. To avoid wave reflections, we should implement a time-dependent radiation (boundary) condition at the lower (wave exit) boundary as in [23].

Our investigation suggests that travelling ionospheric disturbances (SSTIDs, MSTIDs and LSTIDs) of auroral origin are generated by magnetohydrodynamic (MHD) effects.

APPENDIX A. THE CONTINUITY EQUATION AND THE ENERGY EQUATION UNDER THE BOUSSINESQ APPROXIMATION

Taking into account the electromagnetic energy, the equation of conservation of energy for the α-species (or plasma) takes the form

$$\varrho_\alpha \frac{De_\alpha}{Dt} = -\nabla\cdot\mathbf{q}_\alpha - p_\alpha \nabla\cdot\mathbf{u}_\alpha + \omega_\alpha + \nabla\cdot(\mathbf{E}\times\mathbf{H}), \tag{A1}$$

where $\varrho_\alpha \frac{De_\alpha}{Dt}$ represents the internal energy of the α-species per unit of volume and per unit of time, ω_α is the viscous dissipation of the α-species per unit of volume and per unit of time and $\mathbf{q}_\alpha$ is the heat flux vector of the α-species (per unit of area and per unit of time), and as before $\mathbf{E}\times\mathbf{H}$ is the Poynting vector.

At a constant volume, the energy of the ionospheric plasma (α-species) [28] is $e_\alpha = C_{V,\alpha}\,T_\alpha$, where $C_{V,\alpha} = (\partial e_\alpha/\partial T_\alpha)_V$ is the specific heat capacity at constant volume V, and the relation between the pressure p_α, the specific mass ϱ_α and the temperature T_α is the equation of state $p_\alpha = \mathcal{R}_\alpha \varrho T_\alpha$, where $\mathcal{R}_\alpha = C_{p,\alpha} - C_{V,\alpha}$, and $C_{p,\alpha} = (\partial h_\alpha/\partial T_\alpha)_p$ is the specific heat capacity at constant pressure and h_α is the enthalpy of the plasma [16].

We assume that ϱ_α is large enough so that $(Q_\alpha - L_\alpha)M_\alpha \ll \varrho_\alpha$. This assumption is valid in the ionospheric F region where the production rate of the α-species Q_α and their loss rate L_α are almost equal, $Q_\alpha \approx L_\alpha$. In that case, the continuity Equation (2) reduces to

$$\frac{1}{\varrho_\alpha}\frac{D\varrho_\alpha}{Dt} = -\nabla\cdot\mathbf{u}_\alpha. \tag{A2}$$

The goal here is to simplify Eq. (A1) using the Boussinesq approximation. The later approximation is commonly used in the study of geophysical flows, see Spiegel and Veronis [28]. In the governing equations, the fluid density and temperature are assumed to be constant under the Boussinesq approximation, except the terms involving the effects due gravity. The following assumptions are made in the Boussinesq approximation:

(i) The variation of ϱ_α (density) in time and space is small enough so that $\frac{1}{\varrho_\alpha}\frac{D\varrho_\alpha}{Dt} \approx 0$.

(ii) The fluid is almost incompressible or the density does not change much with the pressure p_α, $\frac{\partial\varrho_\alpha}{\partial p_\alpha}$.

(iii) The density varies by only a small amount in the vertical direction.

(iv) The fluid viscosity coefficient μ_α and the thermal conductivity $\mathcal{K}_\alpha$ are assumed to be constant and the viscous dissipation ω_α is negligible.

Thus, the continuity Equation (A2) reduces to $\nabla\cdot\mathbf{u}_\alpha = 0$ under the Boussinesq approximation (assumption 1). Even though this is the case, it cannot be justified to neglect the term $p_\alpha\nabla\cdot\mathbf{u}_\alpha$ in the Equation (A1) because although the term $\nabla\cdot\mathbf{u}_\alpha$ is small, the pressure can be large and the product $p_\alpha\nabla\cdot\mathbf{u}_\alpha$ can be of the same order of magnitude as the other terms in Eq. (A1). Therefore, we keep the

term $p_\alpha \nabla \cdot \mathbf{u}_\alpha$ in Eq. (A1) and rewrite it in terms of ϱ_α and T_α using the continuity Equation (2) and the equation of state of a perfect gas, $p_\alpha = \mathcal{R}_\alpha \varrho_\alpha T_\alpha$.

Next, multiplying both sides of Equation (A2) by the pressure p_α and assuming that the plasma is incompressible yields

$$-p_\alpha \nabla \cdot \mathbf{u}_\alpha = \frac{p_\alpha}{\varrho_\alpha}\frac{D\varrho_\alpha}{Dt} = \frac{p_\alpha}{\varrho_\alpha}\left[\left(\frac{\partial \varrho_\alpha}{\partial T_\alpha}\right)\frac{DT_\alpha}{Dt} + \left(\frac{\partial \varrho_\alpha}{\partial p_\alpha}\right)\frac{Dp_\alpha}{Dt}\right] \approx \frac{p_\alpha}{\varrho_\alpha}\left(\frac{\partial \varrho_\alpha}{\partial T_\alpha}\right)_p \frac{DT_\alpha}{Dt}, \tag{A3}$$

where, as before, the subscript p denotes differentiation of ϱ_α with respect to T_α at constant pressure. Using the equation of state for a perfect gas, Equation (A3) can be written as,

$$-p_\alpha \nabla \cdot \mathbf{u}_\alpha \approx \frac{p_\alpha}{\varrho_\alpha}\left(\frac{\partial}{\partial T_\alpha}\left(\frac{p_\alpha}{\mathcal{R}_\alpha T_\alpha}\right)\right)_p \frac{DT_\alpha}{Dt} = \frac{p_\alpha}{\varrho_\alpha}\frac{p_\alpha}{\mathcal{R}_\alpha}\left(-\frac{1}{T_\alpha^2}\right)\frac{DT_\alpha}{Dt} = -\mathcal{R}_\alpha \varrho_\alpha \frac{DT_\alpha}{Dt}. \tag{A4}$$

Substituting (A4) into the Equation (A1), and using $e_\alpha = C_{V,\alpha}\, T_\alpha$ and $\mathcal{R}_\alpha = C_{p,\alpha} - C_{V,\alpha}$ yields

$$C_{p,\alpha}\, \varrho_\alpha \frac{DT_\alpha}{Dt} = -\nabla \cdot \mathbf{q}_\alpha + \omega_\alpha + \nabla \cdot (\mathbf{E} \times \mathbf{H}), \tag{A5}$$

According to Fourier's law of heat conduction, $\mathbf{q}_\alpha = -\mathcal{K}_\alpha \nabla T_\alpha$, where $\mathcal{K}_\alpha$ is the thermal conductivity. Moreover, under the Boussinesq approximation, the ratio, for instance, of the magnitude of viscous dissipation ω_α to the term $C_{p,\alpha}\, \varrho_\alpha \frac{DT_\alpha}{Dt}$ is very small ($\sim 10^{-7}$) in geophysical flows. This is shown, using dimensional analysis, in Kundu and Cohen [16], p 120. Therefore, the viscous dissipation term in Eq. (A5) is negligible and can be dropped. Thus, substituting $\mathbf{q}_\alpha = -\mathcal{K}_\alpha \nabla T_\alpha$ into Equation (A5), we obtain

$$C_{p,\alpha}\, \varrho_\alpha \frac{DT_\alpha}{Dt} = -\nabla \cdot (-\mathcal{K}_\alpha \nabla T_\alpha) + \nabla \cdot (\mathbf{E} \times \mathbf{H}) = \mathcal{K}_\alpha \nabla^2 T_\alpha + \nabla \cdot (\mathbf{E} \times \mathbf{H}). \tag{A6}$$

Using the incompressibility property (second assumption in the Boussinesq approximation), then $\varrho_\alpha T_\alpha = \varrho_{\alpha,o} T_{\alpha,o} =$ constant, where $\varrho_{\alpha,o}$ and $T_{\alpha,o}$ are some reference density and reference temperature respectively. A slight change in temperature T'_α leads to a slight change in density ϱ'_α. Writting T_α as $T_\alpha = T_{\alpha,o} + T'_\alpha$ and ϱ_α as $\varrho_\alpha = \varrho_{\alpha,o} + \varrho'_\alpha$, where $\varrho'_\alpha \ll \varrho_{\alpha,o}$, $T'_\alpha \ll T_{\alpha,o}$ gives

$$\varrho'_\alpha T_{\alpha,o} + \varrho'_\alpha T'_\alpha + \varrho_{\alpha,o} T'_\alpha = 0. \tag{A7}$$

Neglecting the term $\varrho'_\alpha T'_\alpha$ which is very small in magnitude compared to the other terms since it is a product of perturbation quantities, and using the fact that $\varrho_\alpha - \varrho_{\alpha,o} = \varrho'_\alpha$ and $T_\alpha - T_{\alpha,o} = T'_\alpha$ gives

$$\varrho_\alpha = \varrho_{\alpha,o}\left[1 - \kappa_\alpha (T_\alpha - T_{\alpha,o})\right], \tag{A8}$$

where $\kappa_\alpha = 1/T_{\alpha,o}$ is the thermal expansion.

Thus, using Eq. (A8), the energy Equation (A6) can be written in terms of the density ϱ_α as

$$\frac{D\varrho_\alpha}{Dt} = \mathcal{T}_\alpha \nabla^2 \varrho_\alpha - \frac{\kappa_\alpha}{C_{p,\alpha}} \nabla \cdot (\mathbf{E} \times \mathbf{H}). \tag{A9}$$

This equation can be written in terms of the streamfunction Ψ_α and the density ϱ_α as

$$\varrho_{\alpha_t} - \Psi_{\alpha_z} \varrho_{\alpha_x} + \Psi_{\alpha_x} \varrho_{\alpha_z} - \mathcal{T}_\alpha \nabla^2 \varrho_\alpha = -\frac{\kappa_\alpha}{C_{p,\alpha}} \nabla \cdot (\mathbf{E} \times \mathbf{H}), \tag{A10}$$

where, as before, the subscripts, x, z and t, indicate partial differentiation with respect to x, z, and t, respectively.

REFERENCES

1. Afraimovich, E. L., E. A.Kosogorov, L. A.Leonovich, K. S. Palamartchouk, N. P. Perevalova, and O. M. Pirog, "Observation of large-scale traveling ionospheric disturbances of auroral origin by global GPS networks," *Earth Planets Space*, Vol. 2, 669–674, 2000.
2. Afraimovich, E. L., E. I. Astafieva, and S. V. Voyeikov, "Generation of ionospheric irregularities upon propagation of solitary internal gravity wave during the major magnetic storm of October 29–31, 2003," *Radiophys. Quantum Electronics*, Vol. 49, No. 2, 79–92, 2006.

3. Cannon, P., M. Angling, L. Barclay, C. Curry, C. Dyer, R. Edwards, G. Greene, M. Hapgood, R. Horne, D. Jackson, C. Mitchell, J. Owen, A. Richards, C. Rogers, K. Ryden, S. Saunders, M. Sweeting, R. Tanner, A. Thomson, and C. Underwood, *Extreme Space Weather: Impacts on Engineered Systems and Infrastructure*, Royal Academy of Engineering, London, 2013.
4. Cheng, D. K., *Field and Wave Electromagnetics*, Addison-Wesley Publish Comp. Inc, 1992.
5. Danilov, A. D. and J. Laštovička, "Effects of geomagnetic storms on the ionosphere and atmosphere," *Int. J. Geomagn. Aeron.*, Vol. 2, No. 3, 209–224, 2001.
6. Falconer, D., A. F. Barghouty, I. Khazanov, and R. Moore, "A tool for empirical forecasting of major flares, coronal mass ejections, and solar particle events from a proxy of active-region free magnetic energy," *Space Weather*, Vol. 9, No. 4, S04003, 2011.
7. Figueiredo, C. A. O. B., C. M. Wrasse, H. Takahashi, Y. Otsuka, K. Shiokawa, and D. Barros, "Large-scale traveling ionospheric disturbances observed by GPS dTEC maps over North and South America on Saint Patrick's Day storm in 2015," *JGR Space Phys.*, Vol. 122, No. 4, 4755–4763, 2017.
8. Freidberg, J. P., *Ideal MHD*, Cambridge University Press, 2014.
9. Harris, T. J., M. A. Cervera, and D. H. Meehan, "SpICE: A program to study small–scale disturbances in the ionosphere," *J. Geophys. Res. Space Physics*, Vol. 117, A06321, 2012.
10. Holzworth, R. H., M. C. Kelley, C. L. Siefring, L. C. Hale, and J. D. Mitchell, "Electrical measurements in the atmosphere and the ionosphere over an active thunderstorm, 2. Direct current electric fields and conductivity," *J. Geophys. Res.*, Vol. 19, No. A10, 9824–9830, 1985.
11. Hunsucker, R. D., "Atmospheric gravity waves generated in the high atitude ionosphere: A review," *Rev. Geophys.*, Vol. 20, 293–315, 1982.
12. Hunsucker, R. D. and J. K. Hargreaves, *The High-latitude Ionosphere and Its Effects on Radio Propagation*, Cambridge University Press, 2003.
13. Kelley, M. C. and C. A. Miller, "Electrodynamics of midlatitude spread F, 3. Electrohydrodynamic waves? A new look at the role of electric fields in thermospheric wave dynamics," *J. Geophys. Res.*, Vol. 102, 11539–11547, 1997.
14. King, J. W., "Sun-weather relationships," *Aeronaut. Astronaut.*, Vol. 13, No. 4, 10–19, 1975.
15. Kulsrud, R. M., *Plasma Physics for Astrophysics*, Princeton University Press, 2004.
16. Kundu, P. K. and I. M. Cohen, *Fluid Mechanics*, Academic Press, New York, 2004.
17. Laštovička, J., "Effects of geomagnetic storms-different morphology and origin in the upper middle atmosphere and troposphere," *Stud. Geophys. Geod.*, Vol. 41, 73–81, 1997.
18. Laštovička, J. and A. Bourdillon, "Ionospheric effects on terrestrial communications: Working Group 3 overview," *Ann. Geophys.* Vol. 47, 1269–1277, 2004.
19. Mansilla, G. A. and M. Zossi De Artigas, "Evidence of geomagnetic storm effects in the lower atmosphere: A case study," *Stud. Geophys. Geod.*, Vol. 54, 487–494, 2010.
20. Nijimbere, V., "Ionospheric gravity wave interactions and their representation in terms of stochastic partial differential equations," Ph.D. Thesis, Carleton University, 2014, doi: 10.22215/etd/2014-10245.
21. Nijimbere, V., "Implementation of a Wiener chaos expansion method for the numerical solution of the stochastic generalized Kuramoto-Sivashinsky equation driven by Brownian motion forcing," *Journal of Advances in Applied Mathematics*, Vol. 4, No. 4, 119–142, 2019, doi: 10.22606/jaam.2019.44001.
22. Nijimbere, V. and L. J. Campbell, "Electromagnetic field solutions in an isotropic medium with weakly-random fluctuations in time and some applications in the electrodynamics of the ionosphere," *Progress In Electromagnetics Research B*, Vol. 83, 77–92, 2019.
23. Nijimbere, V. and L. J. Campbell, "A nonlinear time-dependent radiation condition for simulations of internal gravity waves in geophysical fluids," *Appl. Numer. Math.*, Vol. 110, 75–92, 2016.
24. Parks, G. K., *Physics of Space Plasma*, 2nd Edition, Westview Press, 2005.
25. Prikryl, P., S. Hawlitschka, U.-P. Hoppe, S. P. Cannon, and T. P. Bernhard, "Characterizing the ionosphere," Final report of task group IST-051, RTO/NATO, 2009.

26. Ratcliffe, J. A., *An Introduction to the Ionosphere and Magnetosphere*, Cambridge University Press, 1972.
27. Song, Q., F. Ding, W. Wan, B. Ning, and B. Zhao, "Monitoring traveling ionospheric disturbances using GPS network around China during the geomagnetic storm on 28 May 2011," *Science China Earth Sci.*, Vol. 56, 718–726, 2013.
28. Spiegel, E. A. and G. Veronis, "On the Boussinesq approximation for compressible fluid," *Astrophys. J.*, Vol. 6, 442–447, 1960.
29. Sutherland, B. R., *Internal Gravity Waves*, Cambridge University Press, 2010.
30. Torta, J. M., M. Marsal, and M. Quintana, "Assessing the hazard from geomagnetically induced currents to the entire high-voltage power network in Spain," *Earth, Planets and Space*, Vol. 66, No. 87, 2014.
31. Wang, M., F. Ding, W. Wan, B. Ning, and B. Zhao, "Monitoring global traveling ionospheric disturbances using the worldwide GPS network during the October 2003 storms", *Earth Planets Space*, Vol. 59, 407–419, 2007.
32. Zastawniak, T. and Z. Brzeźniak, *Basic Stochastic Processes*, Springer-Verlag, Berlin, 2003.
33. Zhang, S. R., J. M. Holt, P. J. Erickson, L. P. Goncharenko, M. J. Nicolls, M. McCready, and J. Kelley, "Ionospheric ion temperature climate and upper atmospheric long-term cooling," *J. Geophys. Res. Space Physics*, Vol. 121, 8951–8968, 2016.